

INFO8010 - Modeling structural damage for ship collisions against spar floating offshore wind turbines using a deep learning approach

PRISCILLA SALAZAR^a, GABRIEL VANDEGAR^b

^a*lpsalazar@uliege.be (s193098)*

^b*gvandegar@uliege.be (s172877)*

Abstract

This paper presents and compares different approaches to rapidly estimate the elasto-plastic response of a spar Floating Offshore Wind Turbine (FOWT) subjected to ship collision. The wind turbine, idealized as a constant cross-section cantilever tube with a tip mass, is assumed to be struck by a rigid impactor. In the first step, a series of preliminary finite element simulations are performed to build a database and establish the ground truth to train, validate and compare the models. In the second step, observations from the numerical results are used to integrate existing analytical formulations from the literature into a time-stepping algorithm, creating an analytical model. In the third step, a neural network model is developed using a transformer model and trained with the numerical results from the database. Finally, the resulting force-penetration and energy balance curves computed with both models are compared to finite element results. Simulations are performed considering different geometries, impact locations between 25% and 70% of the tower height, and 6000 to 24000-tonne Offshore Supply Vessels (OSVs) approaching at velocities ranging from 0.5 to 5 m/s. The results show that the neural network model provides good approximations in most cases, while the analytical model is limited due to its assumptions.

Keywords: Ship Collisions, Offshore Wind Turbines, Simplified Methods, Finite Element Analysis, Deep Learning

1 Introduction

The advantages of floating offshore wind turbines (FOWT) regarding the exploitation of wind resources in deeper water are well-known to the date. The increase on floating offshore wind pipeline capacity by the end of 2023, shows that this type of technology is reaching the commercial phase, and the global number of floating farms is expected to grow shortly. This expansion would lead to a reduction on navigation space, an increase on traffic flow of service vessels and probably a rearrangement of navigation routes. Consequently, accounting for the risk of ship collisions against offshore wind turbines (OWT) is becoming more relevant during safety assessment. In the most recent events, in April 2023, a cargo ship collided with a wind turbine installed at the Gode Wind1 offshore wind farm (*Orsted's Gode*, 2023). In January 2022, a 37200 tons rudderless cargo ship drifted into the Hollandse Kust Zuid offshore wind farm in the Dutch North Sea during a storm (*Hollandse Kust*, 2023).

During the structural risk assessment, the accidental limit state (ALS) shall be checked not only considering the resistance to the accidental action but also the resistance in damaged condition caused by the accidental action



(a) The cargo ship Petra L. stroke an offshore wind turbine at GodeWind 1 wind farm (Germany). *From (Orsted's Gode, 2023)*



(b) A 37200-tons rudderless cargo ship drifted into the HollandseKustZuid offshore windfarm in the Dutch North Sea. *From (Hollandse Kust, 2023)*

(NORSOK N-001, 2012). Then, it is important to investigate local structural damages that could lead to the loss of integrity or performance of the structure. The analysis of structural damage is studied by different approaches including empirical, experimental, and nonlinear finite element methods (NLFEM). Regarding the study of ship collisions against FOWT, an additional complexity is introduced since environmental loads influence the conditions for the event to occur, and the behavior of both structures during and after the impact.

Echeverry et al. (2019) studied the response of a spar-buoy FOWT collided by a ship using NLFEM software LS-DYNA jointly with MCOL external dynamics solver (*Le Sourne et al., 2007*). The influence of hydrodynamic forces was investigated showing that neglecting hydrodynamic loads led to a significant underestimation of the collision force. *Zhang et al. (2021)* studied the dynamic responses of a spar-buoy FOWT under accidental ship impact considering hydrodynamic, aerodynamic, and mooring loads in the collision model. The study focused primarily on the global motions of a spar FOWT and the resulting acceleration of the nacelle but neglects the deformation of the structure at the impact zone.

Yu et al. (2022) used the nonlinear finite element code USFOS to assess the response of a semisubmersible DTU 10 MW turbine supported by the OO-STAR concrete floater and impacted by a 7500 tons OSV. The approach considers the concrete column strong enough to avoid punching shear or flexural failure, then, only the ship is modeled as a deformable structure.

The abovementioned studies either disregard the structural deformation of the floater due to impact or employ NLFEM commercial software such as LS-DYNA to account for the energy dissipated by deformation and the corresponding contact force. Even when NLFEM approaches allow for a high-fidelity representation of the complex physical phenomena that take place in a ship-FOWT collision event, including large deformations, plasticity, complex contact, and fluid-structure interaction, such numerical analyses remain complex in terms of computation, expertise needed for model preparation and access to software. As an alternative, simplified methodologies to assess the structural damage for steel and concrete FOWT structures have been recently developed.

Marquez et al. (2022) proposed a simplified collision mechanical model to study ship impacts against reinforced concrete FOWTs. The study simulated a collision between a 3000 tons OSV and the ITI Energy barge using LS-DYNA/MCOL. The model correlated well to the nonlinear finite element results in terms of structural penetrations, rigid-body motions, and contact force profiles, with a significantly lower computational cost compared against the nonlinear finite element solutions.

Ladeira et al. (2023) developed a super-element (SE) solver to estimate the force-penetration curve of a standalone tubular OWT support. The approach considers an initial local elastic indentation at the contact zone, followed by a local plastic indentation combined with a global beam-like elastic bending, and a final buckling mechanism at the base of the tube. To simulate the response to impact against a spar-buoy FOWT, *Vandegar et al.* (2024) coupled the aforementioned solver with the rigid-body dynamics solver MCOL.

The use of analytical tool such as the SE solver developed in (*Ladeira et al.*, 2023) offers a good compromise between computational resource, expertise to use the tool and accuracy. However, such tools are limited to certain cases and require many assumptions or simplifications. For instance, the SE solver developed in (*Ladeira et al.*, 2023) neglects the bending of the tower of the FOWT and only considers impact at mid and quarter-length of the tower. Therefore, developing such tool require very tedious work and sometimes require different analytical formulations to treat similar cases with different shape or geometries.

With the recent growth in uses and applications of artificial intelligence, one can't help but wonder if a neural network model could learn to predict the outcome of a collision between a ship and a FOWT. In this paper, the system is highly simplified to enable the performance of numerous numerical simulations in a short period of time, allowing the training of a neural network model to see if it can approximate the outcome of a collision based on a few geometrical parameters.

2 Numerical Model Description and Choice of Parameters

Before developing and training a deep learning model, a database is generated through numerical simulations. The following sections describe the numerical model and outline the steps taken to build and validate it.

Model setup

To generate a large amount of data in a short period of time, the system was highly simplified. In this initial study on the use of deep learning to estimate the outcome of a ship colliding with a spar FOWT, the hydrodynamics of the system are not considered. The ship is simplified as a perfectly rigid wedge, and the ballast of the spar FOWT is also assumed to be perfectly rigid. Consequently, the tower of the FOWT is simplified as a cantilever tube with a tip mass representing the rotor nacelle assembly (RNA) at its free end. Additionally, the FOWT's substructures and superstructures are idealized as a single constant cross-section tube. Put simply, the entire Offshore Wind Turbine is modeled as a cantilever tube with a tip mass, an assumption commonly applied in the structural design of OWTs and fixed offshore platforms alike (*Tong, 2010; Travanca and Hao, 2014*). A representation of an actual FOWT and its simplified model is depicted in Figure 2.

Regarding the simplifications detailed in the previous paragraph, it can be argued that they might lead to an unrealistic reproduction of the OWT's support response. In reality, these structures are generally composed of several tubular components with different cross-sectional properties and internal reinforcements. Additionally, the tower is usually tapered lengthwise, unlike the constant average cross-section adopted for the present models. Nevertheless, even though the applied approach does not strictly replicate the structure's geometry, it is expected to provide a good overview of the response, producing reasonably accurate results.

A detailed study on the numerical model is carried out in *Ladeira et al.* (2023). Briefly, they selected an appropriate experimental impact test from the literature and used it as a reference to calibrate the developed

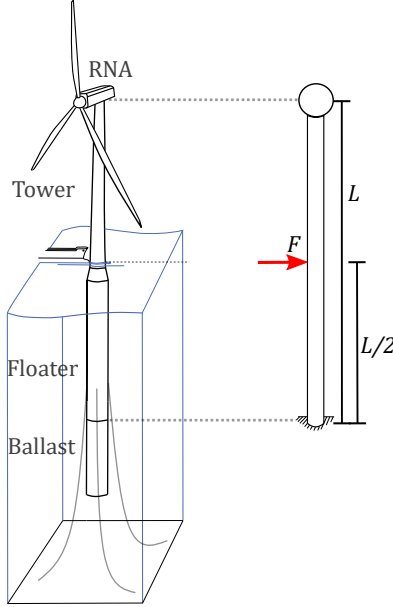
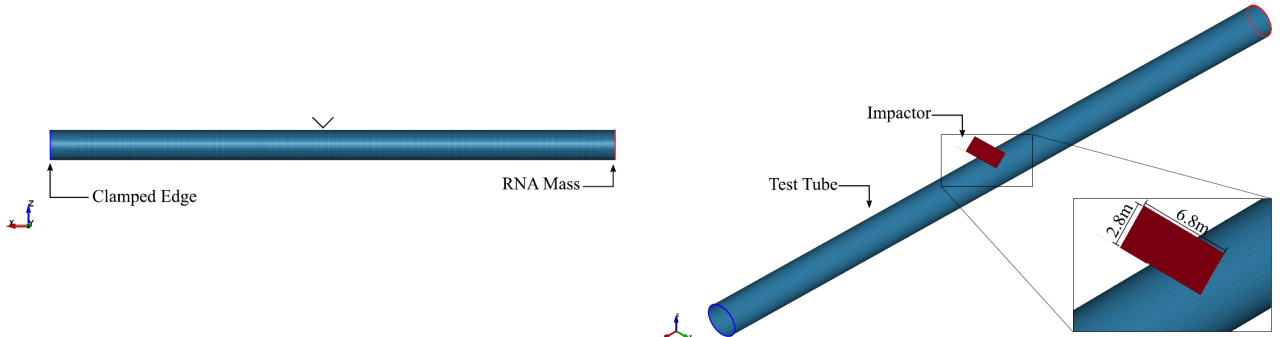


Figure 2: Representation of the FOWT in the SE solver. *From (Ladeira et al., 2023)*

numerical models. For this purpose, the drop tests on tubular members performed by *Cho et al.* (2013) and *Cerik et al.* (2016) were chosen. The experimental setup consists of a simple wedge impactor that was dropped from a predefined height. Depending on the required impact energy, the drop height and the impactor's mass were varied. The test specimens are H-shaped tubular members composed of a main brace connecting two transversal chords, with the components clamped at their extremities. This experimental setup was numerically reproduced using NLFEM on the software LS-DYNA to calibrate the parameters in the numerical simulations.

Using the same modeling parameters as in the experimental setup described above, the numerical model can be set up according to the aforementioned simplifications. In this model, the tube is clamped at one end with a lump mass at its free end. The ship, simplified as a rigid wedge, has a mass m_{ship} and is free to move in one direction, perpendicular to the tower, at an initial velocity v_0 . The model is depicted in Figure 3.



(a) Side view: the clamped base and RNA mass locations are depicted.

(b) Isometric view: a minimum element size of 25 cm and 10 cm was used, respectively, for the tube member and the impactor.

Figure 3: Finite element model setup. *From (Ladeira et al., 2023)*

Concerning the finite element mesh, Belytschko-Tsay elements with two through-thickness integration points are used for the tube, and five points for the impactor. As demonstrated in (*Ladeira et al., 2023*) a mesh size of

25 cm for the tube and 10 cm for the impactor is optimal. A bi-linear piecewise plasticity behavior law is used for the tube, while the impactor is modeled as a rigid material. Strain-rate hardening effects are disregarded due to their uncertainties and modeling complexities, as noted by *Yu and Amdahl (2018)*. Their influence is limited in ship collisions at relatively low velocities (below 10 m/s), as demonstrated by *Cerik & Choung (2020)*.

Results

Three deformation mechanisms can be observed: (i) local crushing, (ii) global bending, and (iii) buckling at the base of the tower (elephant foot buckling). The first deformation mechanism, local crushing, can last from the beginning to the end of contact between the ship and the tower, or it can stop after the ship reaches a maximum penetration δ^* , which highly depends on the tower geometry and the ship's initial velocity. Simultaneously, the second deformation mechanism can occur, usually for a short period, and may then be followed by the elephant foot buckling. However, the third deformation mechanism, the elephant foot buckling, is usually not observed for collision with ships traveling at low initial velocities (below 3 m/s). The deformation mechanisms are depicted in Figure 4 for the actual model of a platform.

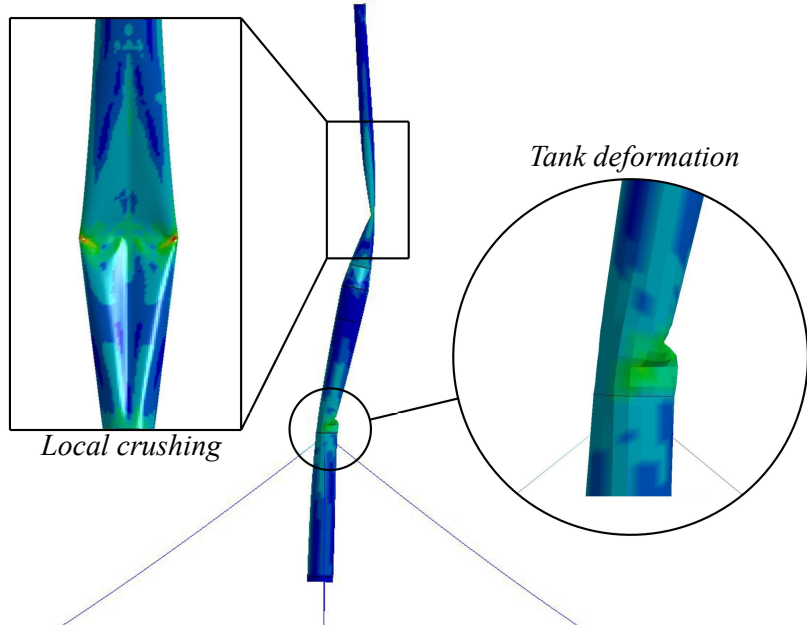


Figure 4: Deformation mechanism of a spar type FOWT. Numerical simulation of a 6000-tonnes OSV colliding into a OC3-Hywind platform at 5m/s. *From (Echeverry, 2021)*

As can be seen in Figure 5, similar deformations are observed in the simplified model. This numerical model represents the Damiani 5MW (*Ng and Ran, 2016*), simplified as a tube with a length of 120 m, a diameter of 5.8 m, a wall thickness of 37 mm, and a tip mass of 350 tons. In addition, the mechanical properties of steel are constant throughout the tube and are as follows: a steel density of 8500 kg/m^3 , a yield stress of 363.7 MPa, and a Young's modulus of 207 GPa.

In addition, the history plot of the force, kinetic and internal energies, and the local, global, and overall penetrations are given in Figure 6. In this paper, the local penetration refers to the variation of the distance between the point at the center of the contact region and its diametrically opposite node, representing the crushing of the tube. The global penetration is the displacement measured at the point opposite to the contact

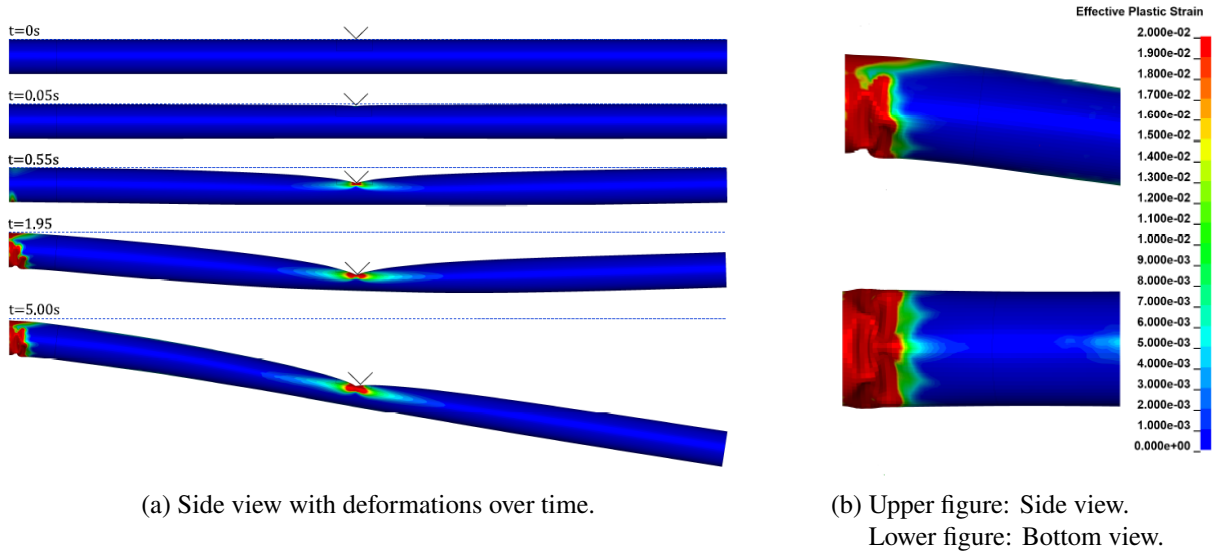


Figure 5: Evolution of the collision process over time for an impact at 5m/s at mid-length, and closer view of the elephant foot buckling with color mapping display of effective plastic strain. *From (Ladeira et al., 2023)*

region, representing the deflection of the tube. The overall penetration is the sum of the local and global penetrations, which also represents the ship's displacement. These history plots are the output that will be estimated using the super element approach and the deep learning approach.

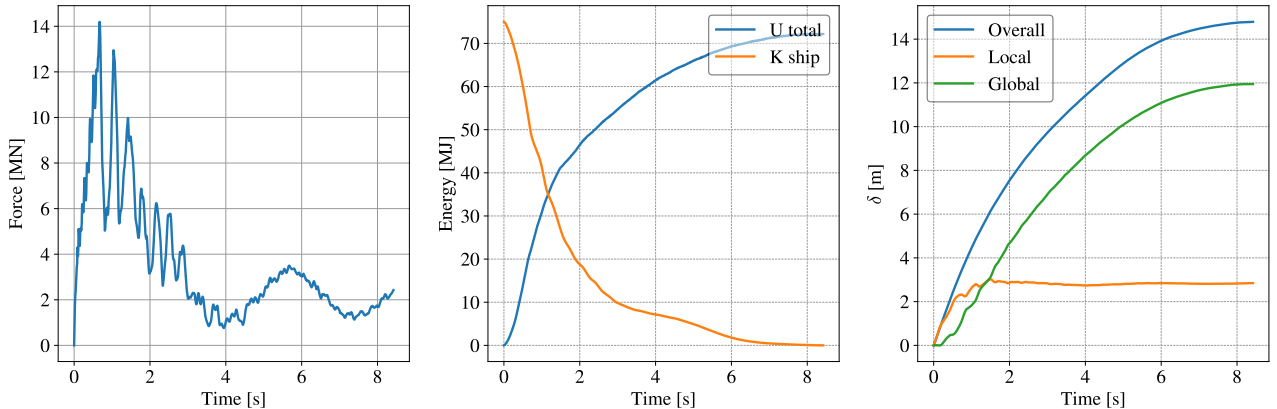


Figure 6: Deformation mechanism of a spar type FOWT. Numerical simulation of a 6000-tonnes OSV colliding into a OC3-Hywind platform at 5m/s. *From (Echeverry, 2021)*

Choice of parameters

The numerical simulations were performed using LS-DYNA, where the commands governing the simulation can either be managed through the graphical user interface (GUI) or directly through a text file. By creating the model outside the GUI, it can be parameterized, allowing for the easy generation of numerous simulations. Such parameterized modeling can be done using GMSH (*Geuzaine et al., 2009*), enabling a large number of simulations to be performed over a few days.

A fairly naive approach was used to generate the inputs for each simulation. Basically, each input is delimited

by a certain range, and for each simulation, its inputs are selected at random within their respective ranges. The main motivation for using this approach is to demonstrate that the presented models not only work for specific configurations with specific aspect ratios but also perform well across a wide range of geometries, even though some of them may not be technically feasible.

To define the range for each input, a study on deployed and in-development standalone and floating offshore wind turbines was conducted, as well as a review of the recommended practices provided by classification societies, such as *Veritas (2010)*. The ranges for each input are summarized in Table 1. For each simulation, the inputs are: the radius of the tube, the thickness of the tube, the length of the tube, the mass of the rotor nacelle assembly, the yield stress of the tube, the initial impactor velocity, the mass of the impactor, and the impact position given as a percentage of the length of the tube. These inputs are denoted as R , t , L , m_{RNA} , σ_y , v_{ship} , m_{ship} , and h , respectively.

Table 1: Choice of the parameters used to generate the dataset

	R [m]	t [mm]	L [m]	m_{RNA} [tons]	σ_y [MPa]	v_{ship} [m/s]	m_{ship} [tons]	h [%]
min	2.5	30	100	272	235	0.5	6000	25
max	5	60	200	820	390	5	24000	70

3 Simplified Analytical Method

To keep this report short, the analytical development of the simplified model is not details herein. Please refer to *Ladeira et al. (2023)* for detailed development.

4 Neural Network Approach

In this project, a Transformer-based deep learning model is developed and trained to estimate a sequence of outputs based on a set of input features. The following sections outline the steps taken to implement, train, and validate this model.

Task definition

The aim of the deep learning model is to estimate the history plot of the force, energy, and penetration of the ship into the FOWT's tower from a few inputs. Simply put, the model's goal is to estimate the diagrams presented in Figure 6 given the inputs specified in Table 1.

To achieve this, the outputs are structured as sequences, with each sequence consisting of 201 equally spaced points representing the time domain between 0 and 10 seconds. This approach ensures that the temporal evolution of the force, kinetic energy of the ship, internal energy of the FOWT, overall penetration, local penetration, and global penetration is captured comprehensively over the duration of the event.

Model architecture

Initially, various model architectures were investigated, including simple multilayer perceptrons (MLP), recurrent neural networks (RNN), and Transformers. However, the transformer model outperformed both the MLP and RNN models, even with a smaller dataset and less parameter tuning. Therefore only the transformer model will be presented in this report.

The Transformer architecture introduced in *Vaswani et al. (2017)* is the base of the model. This architecture is renowned for its effectiveness in handling sequential data, particularly in the context of natural language processing. However, its versatility makes it suitable for various other applications, including sequence estimation task.

The model comprises several key components. Firstly, an embedding layer transforms the input features into a higher-dimensional space suitable for the Transformer. Since the Transformer lacks an inherent sense of order, positional encoding is added to the embedded inputs to provide information about the position of each element in the sequence. The core of the model is the Transformer encoder, which consists of multiple encoder layers containing multi-head self-attention mechanisms and feed-forward neural networks. These layers capture the relationships between different elements in the sequence. Finally, linear decoder layers transform the encoded representations into the six output sequences.

Training Process

To train the Transformer model, a standard supervised learning procedure is followed. The steps involved in the training process are:

1. Data Preparation: Approximately 1000 numerical simulations were conducted using LS-DYNA to generate the necessary data¹. The dataset was then organized into input-output pairs and was stored in an SQLAlchemy database for efficient retrieval and management.
2. Normalization: Both input and output data are normalized to ensure numerical stability during training. The inputs are scaled to a standard range between 0 and 1 such that:

$$input^* = \frac{input - min}{max - min} \quad (1)$$

where $input^*$ denotes the normalized input, min and max are the minimum and maximum values of the input as specified in Table 1, respectively, and $input$ is the original input.

And the outputs are normalized based on the inputs:

$$F^*(t) = \frac{F(t)}{\frac{m_{pl}}{Lh}} \quad (2)$$

$$E^*(t) = \frac{E(t)}{\frac{1}{2}m_{ship}v_{ship}^2} \quad (3)$$

$$\delta^*(t) = \sqrt{\frac{\delta(t)g}{v_{ship}^2}} \quad (4)$$

¹The computer used for the numerical simulation and the training of the model has the following configuration: an AMD Ryzen 9 5900X processor with 12/24 cores and an NVIDIA RTX 3050 GPU with 8 GB of DDR6 memory.

In Equation 2, the force is normalized using the maximum force in bending, where F and F^* denote the original output force and the normalized force respectively, $m_{pl} = \frac{4}{3}\sigma(R^3 - (R-t)^3)$ is the maximum plastic moment of the tube in bending, and Lh is the arm lever.

In Equation 3, the energy is normalized using the initial kinetic energy brought to the system (both the kinetic and internal energies are normalized with this equation).

In Equation 4, The penetration is normalized using the Froude number (the overall, local, and global penetration are normalized with this equation).

3. Training Loop: The training loop iterates over the dataset for a specified number of epochs. In each iteration, the model's parameters are updated to minimize the loss function, which in this case is the Mean Squared Error (MSE) between the predicted and actual sequences.

Smoothing the Output

To ensure the predicted sequences are smooth and free from abrupt jumps, a low-pass filter is applied to the model's output. This filtering step is useful for maintaining the physical plausibility of the predictions, especially when dealing with time-series data. The low-pass filter effectively removes high-frequency noise from the predictions, resulting in smoother output sequences.

Evaluation

The trained Transformer model is evaluated using the coefficient of determination, commonly referred to as R^2 , to quantify its performance. The R^2 score provides an intuitive measure for the model's predictions. By calculating the R^2 score for each sequences, a comprehensive measure of the model's accuracy is obtained. This score is computed as follows:

$$R^2 = 1 - \frac{\sum_{i=1}^n (A_i - F_i)^2}{\sum_{i=1}^n (A_i - \bar{A})^2} \quad (5)$$

where n is the number of items in the sequence, A_i is the actual value, F_i is the value predicted by the model, and \bar{A} is the mean of the actual values.

Then, the R^2 score is adjusted to yield a score between 0 and 100, where 0 indicates a poor approximation and 100 signifies a perfect match:

$$SCORE = \max(R^2, 0) \cdot 100 \quad (6)$$

The Adam optimizer is used to train the model with a learning rate of 0.0001 and the following parameters: 1000 epochs, 100 hidden layers, a batch size of 32, 10 layers, 10 heads, and a dropout rate of 0.2. The convergence of the loss and the score for each sequence is presented in Figure 7, showing that the loss converges after approximately 200 epochs. However, it is noted that the score for each sequence does not converge at the same rate, nor do they all reach a perfect score.

Finally, a few example results are presented in Figure 8, with their inputs listed in Table 2 and scores in Table 3. The model generally provides good approximations for penetration and energy values. However, the approximations for force and local penetration are more case-sensitive due to the eigenmodes of the tubes, both in bending and circumferential deformation. In addition, as this is a preliminary study, the scores might not be

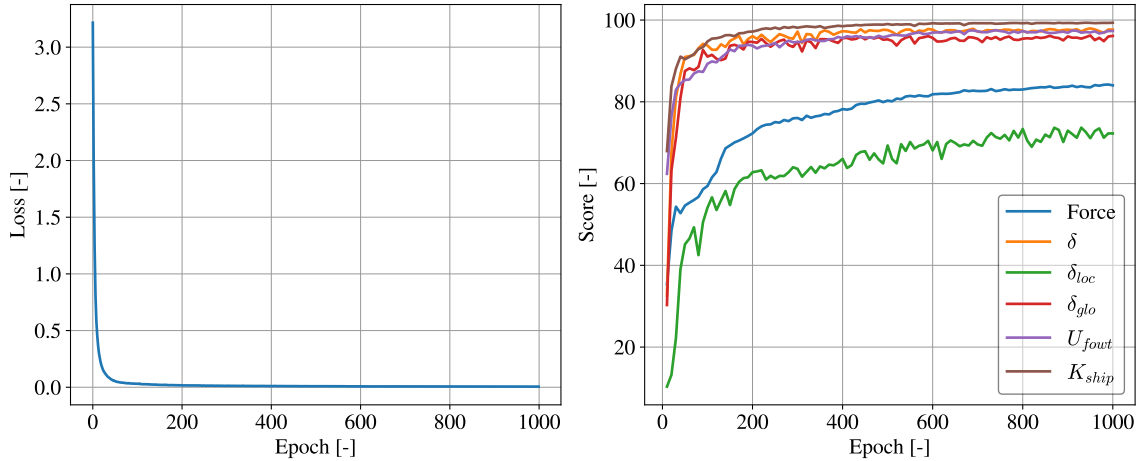


Figure 7: Convergence rate of the model. Left: convergence of the loss; Right: convergence of each sequence.

computed as accurately as possible. For instance, in cases one and two, contact is lost before the end of the sequence. However, the NN model is not yet capable of stopping the sequence accordingly, which may bias the computed scores due to extra values added to the numerical results to reach the proposed sequence length. In practice, when computing the loss and score, values after the loss of contact between the impactor and the tube should be discarded, leaving room for improvement in this study.

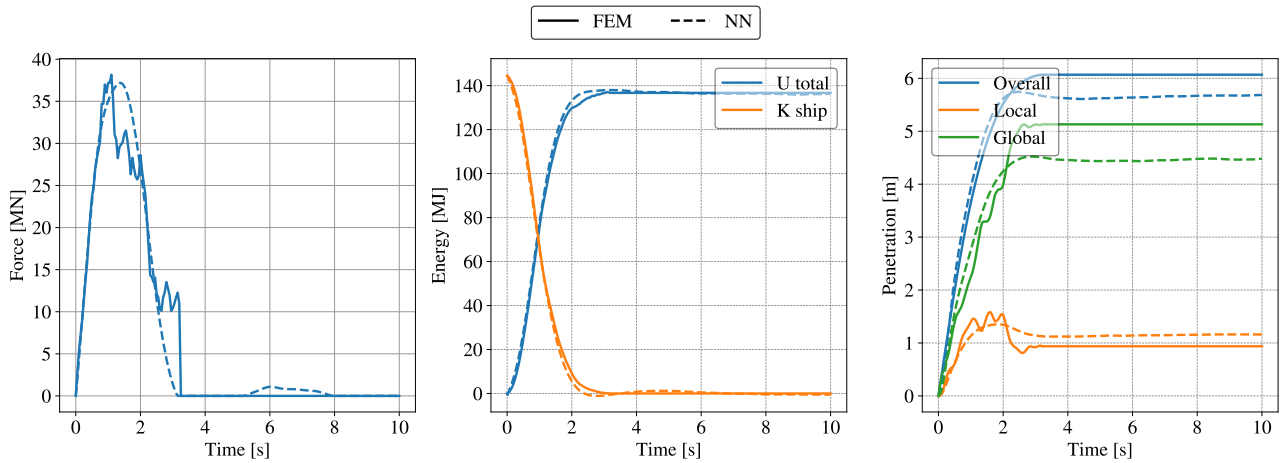
Table 2: Input data for different test samples with randomly distributed inputs.

Test ID	R [m]	t [mm]	L [m]	m_{RNA} [tons]	σ_y [MPa]	v_{ship} [m/s]	m_{ship} [tons]	h [%]
1	4.4	33	179	468	299	4.1	10289	57
2	4.8	56	123	337	310	3.7	13139	28
3	3.1	48	175	575	271	1.3	14444	33

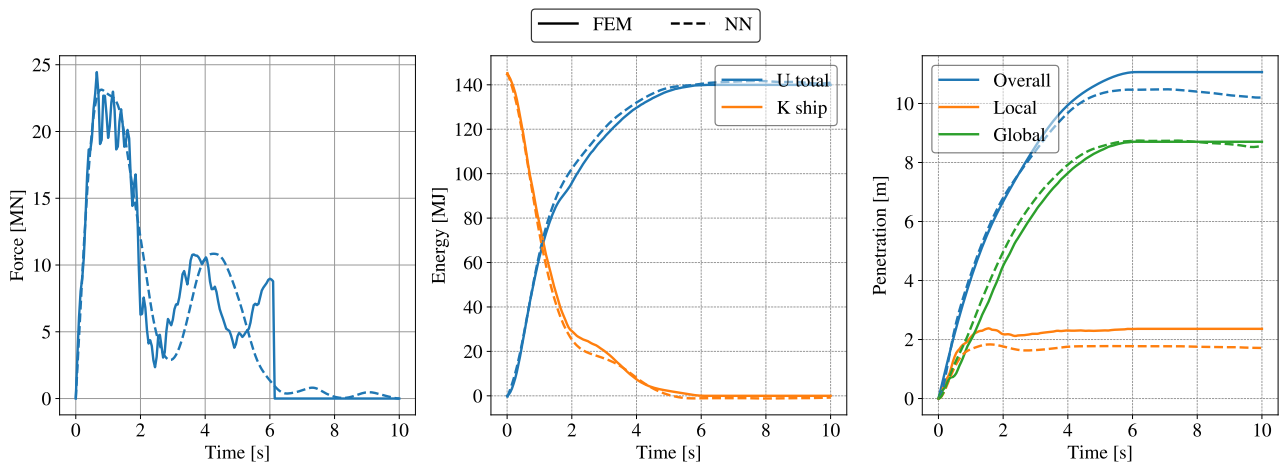
Table 3: Score in percent computed for different test samples with randomly distributed inputs.

ID	Force	δ	δ_{loc}	δ_{glo}	U_{fowt}	K_{ship}
1	81.1	98.7	50.8	99.1	99.3	98.9
2	89.0	97.5	98.5	93.5	98.6	99.8
3	92.7	91.4	0.0	93.2	99.9	99.8

(a) Test 1



(b) Test 2



(c) Test 3

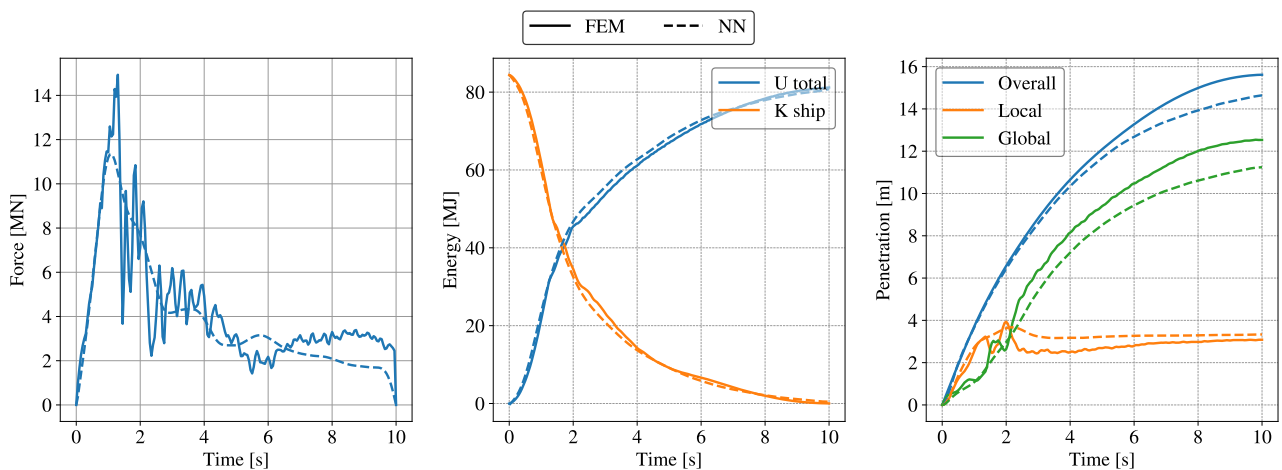


Figure 8: Comparison of the history plot of the force, energy balance, and penetration obtained numerically and with the neural network model for different test samples with randomly distributed inputs.

5 Results and Comparison Between the Models

This section presents a comparison between the super element (SE) model and the neural network (NN) model. To demonstrate the NN model with realistic inputs and to remain within the applicable range of the SE model, the seven OWT configurations selected in *Ladeira et al. (2023)* are used for comparison. Additionally, since the SE model is constrained to impacts at mid-length and quarter-length, the comparison between the two models focuses on impacts at mid-length with initial impactor velocities of 2m/s and 5m/s. The dimensions of the selected OWTs, which serve as inputs for each model, are detailed in Table 4.

Table 4: Selected OWT support structures in *Ladeira et al. (2023)* and their main dimensions. Seven test models covering a range of 5MW to 15MW OWTs are defined.

Model	R [m]	t [mm]	L [m]	m_{RNA} [tons]	σ_y [MPa]	m_{ship} [tons]	h [%]
1 Damiani 5MW	2.9	37	120	350	363	6000	50
2 DOWEC 6MW	2.65	47	110	272	363	6000	50
3 DTU 10MW	4.2	60	145	675	363	6000	50
4 IEA Wind 15MW	4.15	40	180	820	363	6000	50
5 NREL 5MW OC3	3.5	39	140	350	363	6000	50
6 Hywind Scotland 6MW	4.5	60	160	350	363	6000	50
7 Hywind Tampen 8MW	3.6	40	105	480	363	6000	50

Furthermore, the SE model, in addition to its limitations regarding quarter-length and mid-length impacts, cannot distinguish between local and global penetrations, posing challenges for accurate assessments.

Finally, in these comparisons, the R^2 score is computed using only the values in the sequence until the loss of contact is observed in the numerical simulation. This approach ensures that the extra values computed by the NN are discarded, preventing them from biasing the final score.

2ms

The comparison of the scores for an impactor colliding with a velocity of 2m/s with the selected OWTs aforementioned are presented in Table 5. The computed history plots up until the loss of contact between the ship and the OWT are shown in Figure 9. As can be seen, both models give good results in general, but the NN model seems to perform better overall. Furthermore, although the NN model can compute both local and global penetration, the approximations obtained are not yet reliable. Therefore, further work is needed to improve the accuracy of the penetrations computed by the NN model.

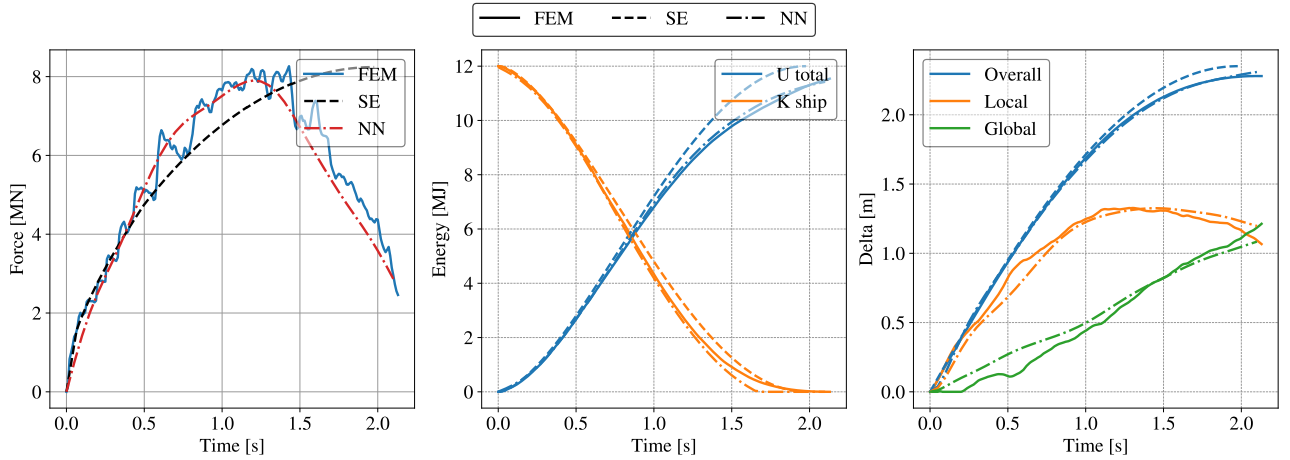
5ms

The comparison of the scores for an impactor colliding with a velocity of 5m/s with the selected OWTs aforementioned are presented in Table 6. The computed history plots up until the loss of contact between the ship and the OWT are shown in Figure 10. As can be seen, the NN model outperform the SE model for the force computation and gives better approximation in all the other cases. In addition, the local and global penetration are generally well approximated at this impactor velocity.

Table 5: Comparison of the R^2 score computed for the super element model and the neural network model for a 2m/s mid-length impact.

Model	Force		δ		δ_{loc}		δ_{glo}		U_{fowt}		K_{ship}	
	SE	NN	SE	NN	SE	NN	SE	NN	SE	NN	SE	NN
1	16.2	94.5	99.7	99.7	-	96.2	-	90.6	97.4	99.9	99.5	99.8
2	0.0	89.7	99.7	99.1	-	71.2	-	92.7	90.8	99.3	99.9	99.2
3	94.5	91.1	99.3	94.2	-	60.2	-	0.0	94.1	96.6	99.8	97.7
4	91.2	34.7	99.9	98.1	-	37.6	-	0.0	96.6	99.5	99.9	98.7
5	82.9	85.3	99.7	99.6	-	96.0	-	71.5	98.2	99.7	99.4	99.9
6	78.1	88.6	99.4	95.9	-	60.5	-	0.0	90.0	97.9	99.9	98.0
7	71.2	71.6	99.4	99.0	-	90.8	-	0.0	98.8	99.6	97.7	99.9
Average	62.0	79.4	99.6	98.0	-	73.2	-	36.4	95.1	98.9	99.4	99.0

(a) Model 1



(b) Model 2

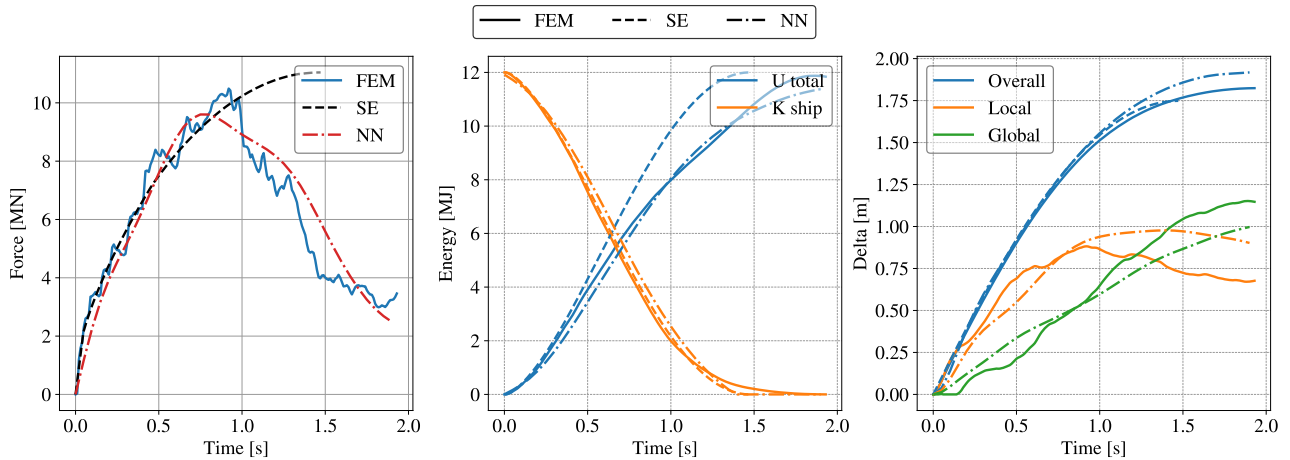
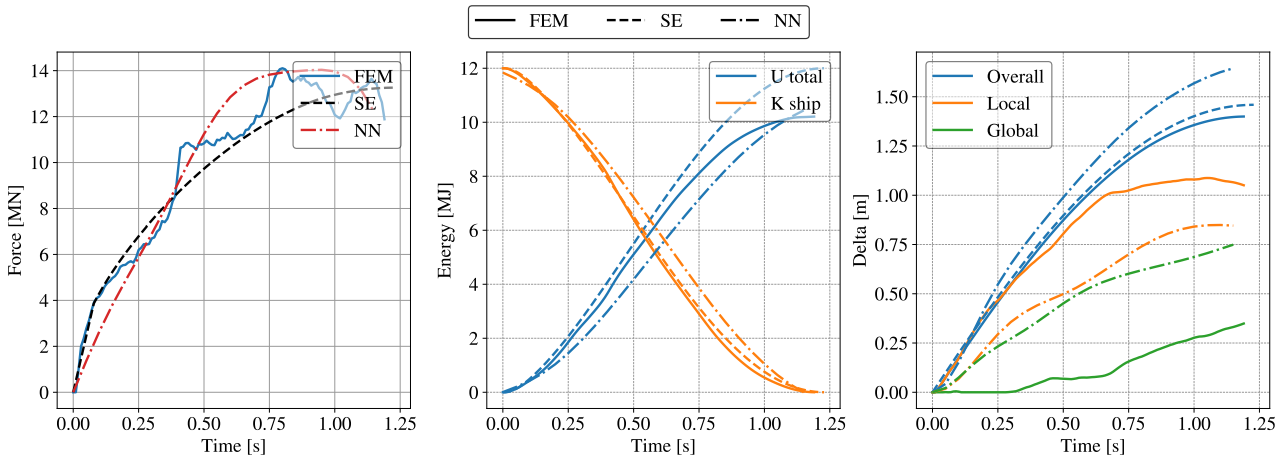
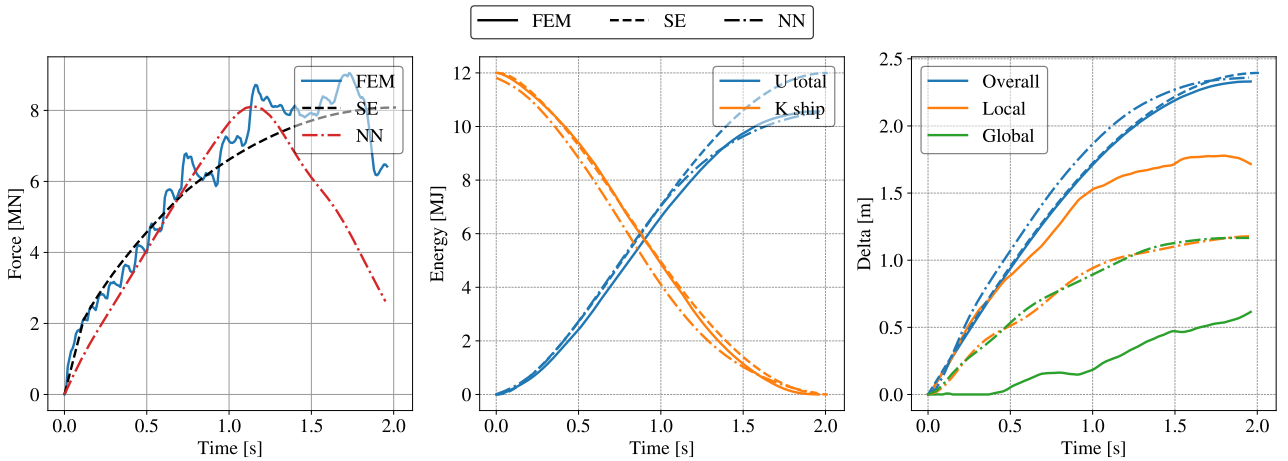


Figure 9: Comparison of the history plot of the force, energy balance, and penetration obtained numerically, with the super element model and with the neural network model for a 2m/s impact at mid-length.

(c) Model 3



(d) Model 4



(e) Model 5

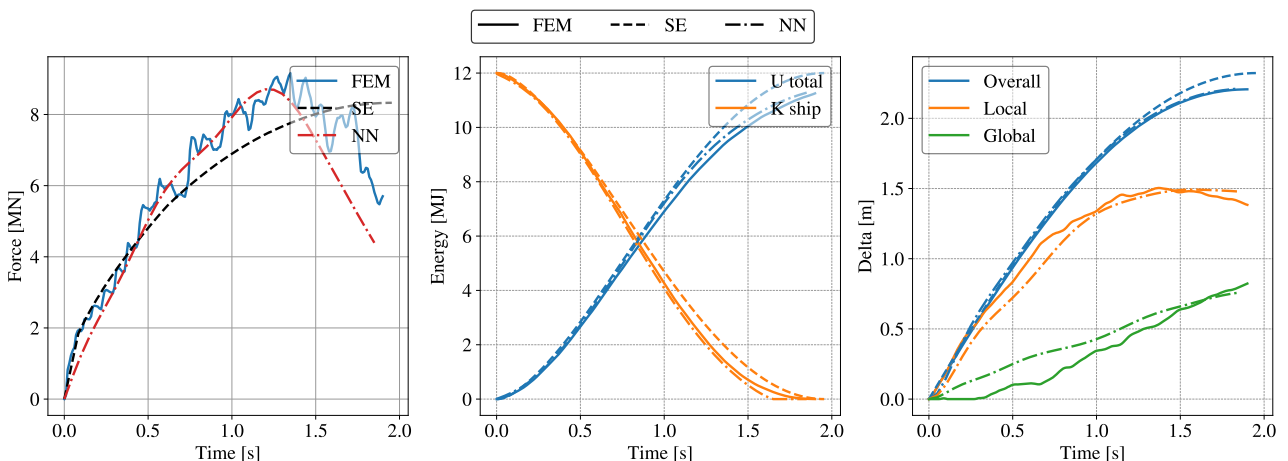
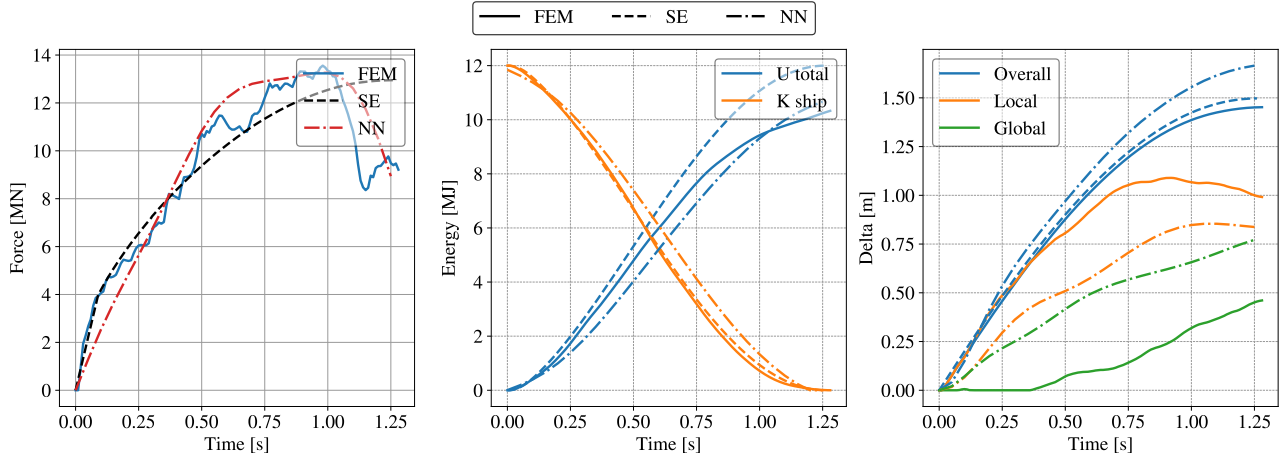


Figure 9: Comparison of the history plot of the force, energy balance, and penetration obtained numerically, with the super element model and with the neural network model for a 2m/s impact at mid-length.

(f) Model 6



(g) Model 7

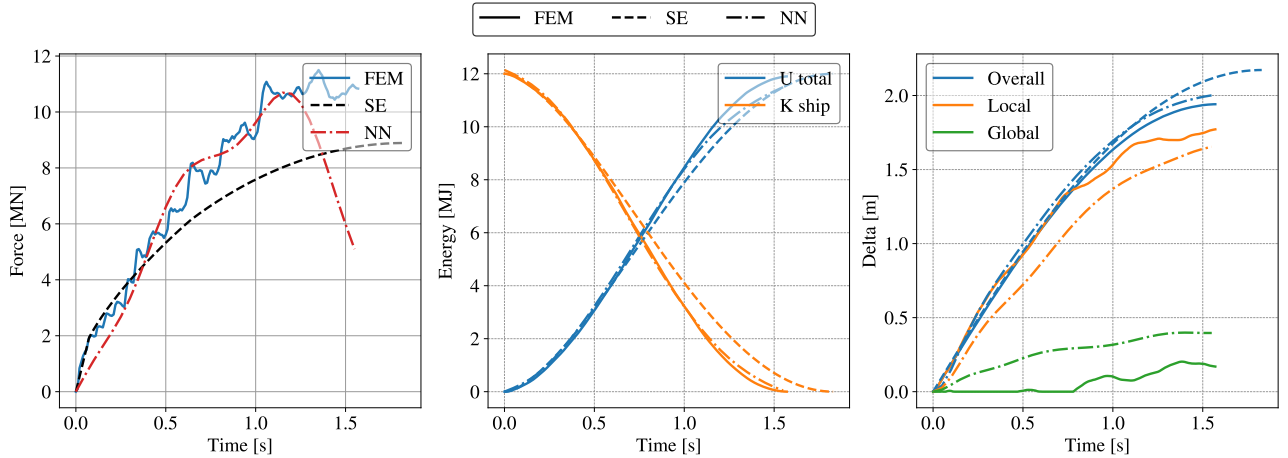
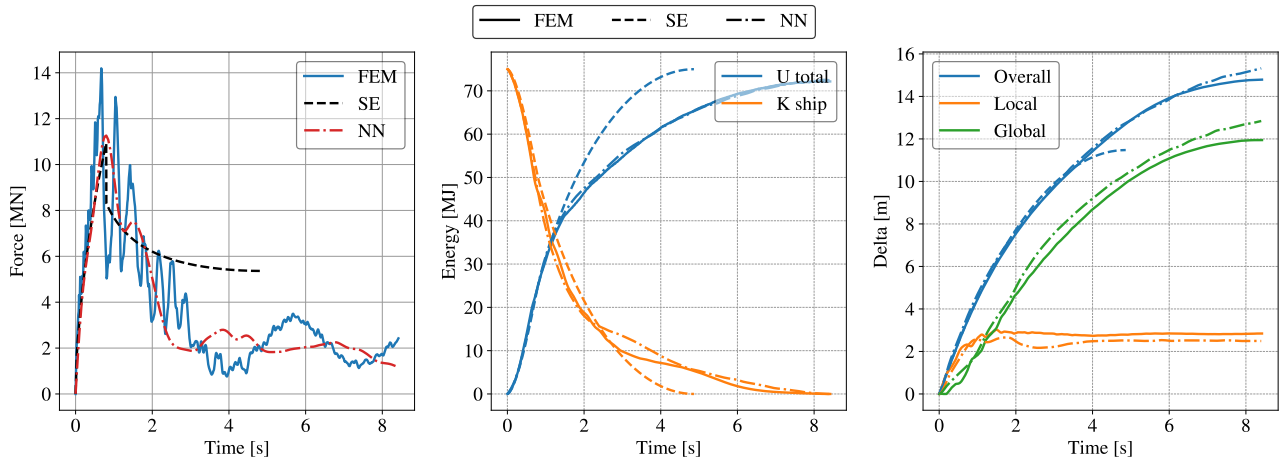


Figure 9: Comparison of the history plot of the force, energy balance, and penetration obtained numerically, with the super element model and with the neural network model for a 2m/s impact at mid-length.

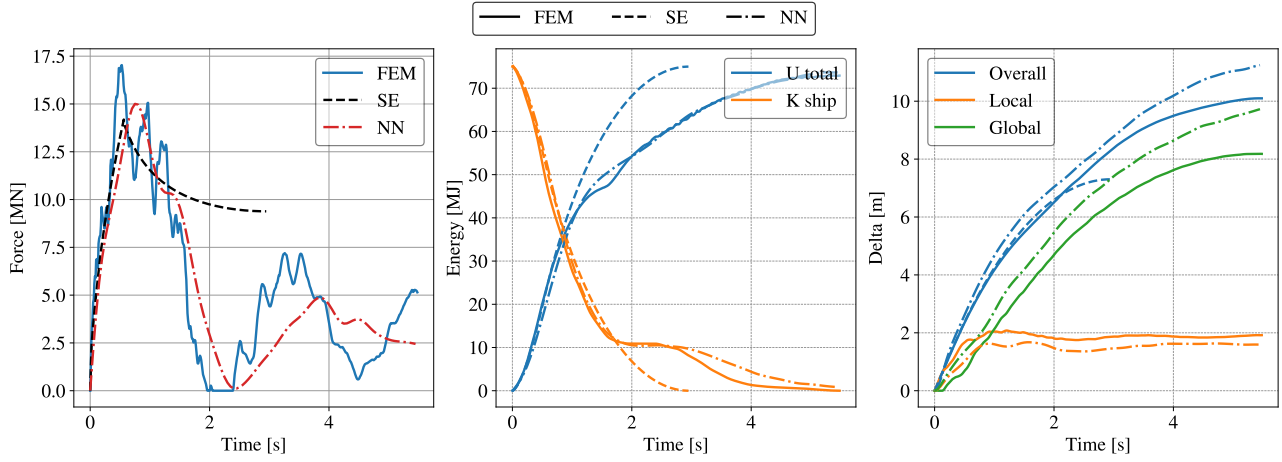
Table 6: Comparison of the R^2 score computed for the super element model and the neural network model for a 5m/s mid-length impact.

Model	Force		δ		δ_{loc}		δ_{glo}		U_{fout}		K_{ship}	
	SE	NN	SE	NN	SE	NN	SE	NN	SE	NN	SE	NN
1	0.0	71.2	89.9	99.8	-	59.4	-	98.1	84.3	99.9	97.4	99.3
2	0.0	73.6	83.7	97.0	-	12.2	-	92.4	81.6	99.6	95.3	98.9
3	23.7	87.9	98.4	81.1	-	89.8	-	11.3	97.3	96.8	96.5	96.5
4	0.0	84.6	96.2	98.1	-	78.2	-	94.7	87.6	98.7	99.2	99.6
5	0.0	77.5	92.8	99.0	-	82.0	-	95.4	86.1	99.8	98.1	99.8
6	0.0	82.8	98.5	87.5	-	88.0	-	28.2	97.6	97.2	97.1	96.4
7	0.0	84.6	97.4	96.1	-	88.7	-	83.9	92.3	99.7	97.6	99.4
Average	3.4	80.3	93.8	94.1	-	71.2	-	72.0	89.5	98.8	97.3	98.6

(a) Model 1



(b) Model 2



(c) Model 3

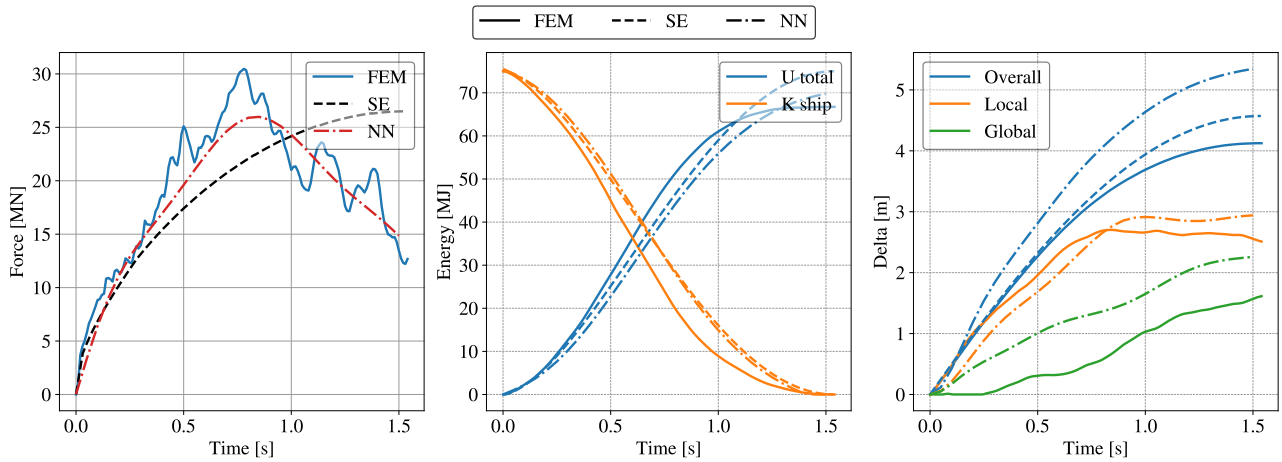
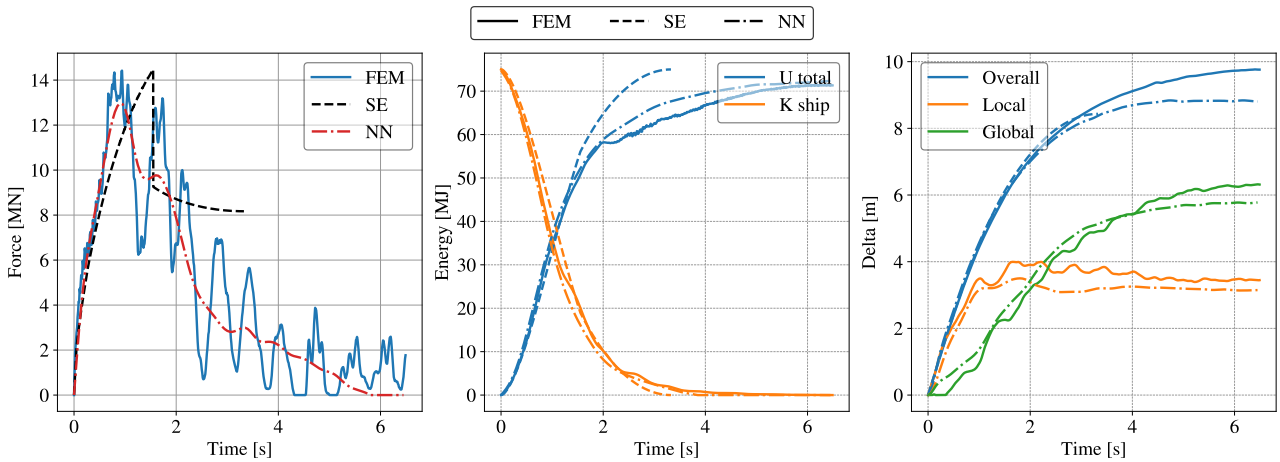
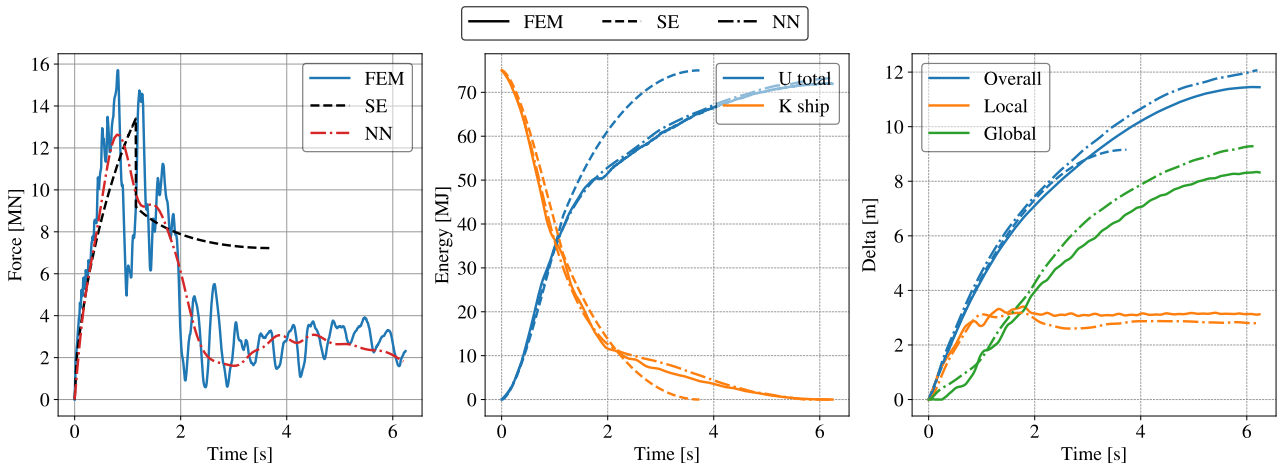


Figure 10: Comparison of the history plot of the force, energy balance, and penetration obtained numerically, with the super element model and with the neural network model for a 5m/s impact at mid-length.

(d) Model 4



(e) Model 5



(f) Model 6

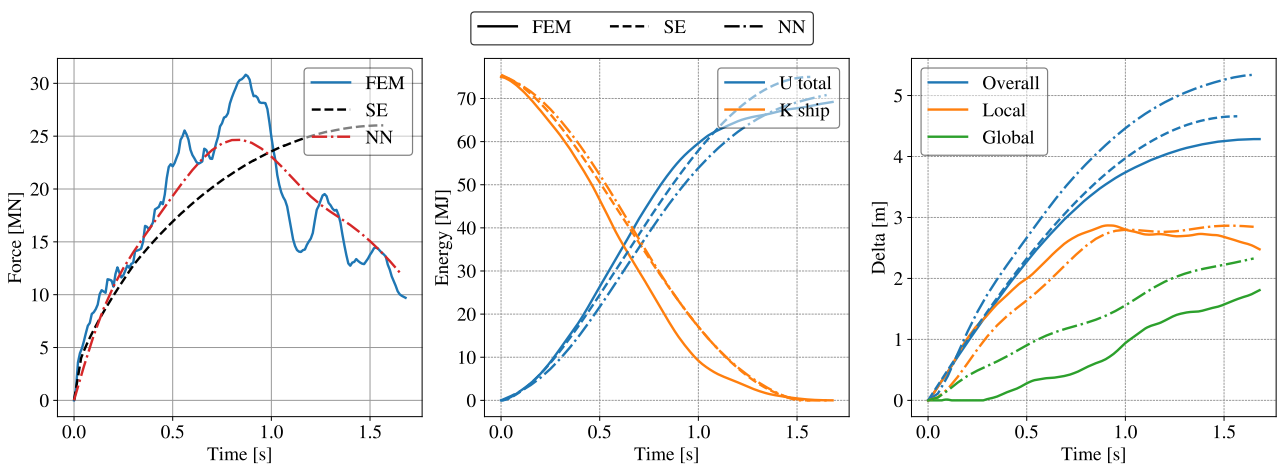


Figure 10: Comparison of the history plot of the force, energy balance, and penetration obtained numerically, with the super element model and with the neural network model for a 5m/s impact at mid-length.

(g) Model 7

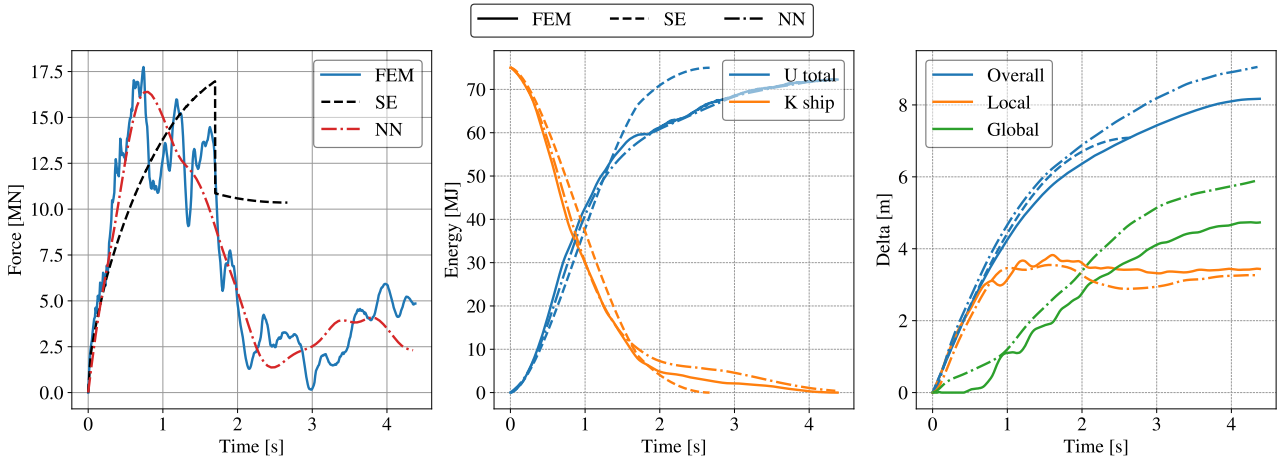


Figure 10: Comparison of the history plot of the force, energy balance, and penetration obtained numerically, with the super element model and with the neural network model for a 5m/s impact at mid-length.

Practical comparison of the models

As it can be seen from the results, the NN model generally performs better than the SE model. Additionally, the NN model has fewer simplifications and fewer restrictions compared to the SE model. For example, the NN model can compute impacts along the length of the tower, while the SE model is limited to mid-length impacts. More generally, the limitations of the NN model are those of the numerical model used to train it, whereas the limitations of the SE model arise from the application range of the analytical formulation used in the model, which is more restricted.

However, it is important to note that the NN model is trained with NLFEM numerical results. Therefore, the model is at most as accurate as the numerical model. Consequently, the main reliability of the NN model depends on the reliability of the numerical simulations. Additionally, the NN model functions as a black box, while the SE model is developed with physics-based analytical formulas that work together in a logical and comprehensive algorithm.

Finally, a large database is required to train the NN model. In this study, the numerical model was highly simplified to generate numerous simulations in a short amount of time. These simplifications align with those made to the SE model, allowing for a more objective comparison of results. However, the NN model should ideally be trained with more realistic collision simulations, which would significantly increase the computational cost to generate the necessary training database.

The main advantages and drawbacks are summarized in Table 7.

Table 7: Summary of the advantages and drawbacks of each model.

	NN	SE
Advantage	<ul style="list-style-type: none"> • Better approximation • Easy to set up • Wider range of application 	<ul style="list-style-type: none"> • Physics-based algorithm • Comprehensive and logical algorithm
Drawback	<ul style="list-style-type: none"> • Black box • Based on numerical results 	<ul style="list-style-type: none"> • Hard to set up • Smaller range of application

6 Conclusion

The offshore wind energy industry is experiencing rapid growth as the world transitions to decarbonized energy production. However, this expansion poses a significant challenge for maritime safety due to the increased risk of collisions between ships and OWTs, either passing by or actively approaching for maintenance operations.

To ensure the crashworthiness of these structures, engineers commonly use NLFEA, which allows for accurate modeling of the complex phenomena involved in ship-OWT collision events. Although reliable and precise, NLFEA can be computationally expensive and impractical for applications requiring numerous simulations of different collision scenario, such as pre-project risk assessments, probabilistic damaged stability analyses, and structural optimization routines. In these situations, simplified approaches that balance accuracy and computational cost become essential.

In this paper, two simplified approaches were presented: one based on analytical formulations and the other employing a deep learning model trained with numerical results. The comparative analysis showed that the deep learning approach generally provides better results than the analytical approach. However, it must be pointed out that the deep learning approach functions as a black box, and therefore, its reliability might be questioned.

Perspective and Future Works

In this paper, the NN model was trained with a naive generation of numerical simulations. For future work, it would be valuable to compare the model when trained with realistic geometrical ratios. Additionally, the normalization proposed for the penetration might not be optimal. Investigating a better method to normalize the penetration could result in more consistent scoring for all outputs.

The outputs computed by the NN model in this paper are the same as those for the SE model. However, the general idea of the SE model is to develop a force-penetration diagram and then compute the force and energies using a quasi-static approach in a time-stepping algorithm. This approach makes the SE model very powerful when coupled with other tools, as demonstrated in *Marquez et al. (2022)*, *Vandegar et al. (2023)* and *Salazar et al. (2024)*. Therefore, instead of computing the history plots, the NN model should compute force-penetration and local/global penetration-penetration relationships to couple this NN model with other external solvers such as MCOL or, later on, with a model computing the deformation of the impactor.

Lastly, the history of the deformed nodes could also be estimated by the model to reconstruct the deformation of the tube over time in a 3D model.

Bibliography

- Cerik, B. C. and Choung, J. (2020). On the modelling of strain-rate effects in nonlinear fe analysis of ship collisions. In *Proceedings of the International Conference on Ships and Offshore Structures, Glasgow*.
- Cerik, B. C., Shin, H. K., and Cho, S. R. (2016). A comparative study on damage assessment of tubular members subjected to mass impact. *Marine Structures*, 46:1–29.
- Cho, S., Seo, B., Cerik, B., and Shin, H. (2013). Experimental and numerical investigations on the collision between offshore wind turbine support structures and service vessels. *Collision and grounding of ships and offshore structures*. CRC Press/Taylor and Francis Group, London, pages 281–288.
- Echeverry, S. (2021). *Numerical and analytical study of a spar-like floating offshore wind turbine impacted by a ship*. PhD thesis, University of Liege. Funded by FRIA.
- Echeverry, S., Márquez, L., Rigo, P., and Le Sourne, H. (2019). Numerical crashworthiness analysis of a spar floating offshore wind turbine impacted by a ship. In *Developments in the collision and grounding of ships and offshore structures*, pages 85–95. CRC Press.
- Geuzaine, C. and Remacle, J.-F. (2009). Gmsh: A 3-d finite element mesh generator with built-in pre- and post-processing facilities. *International Journal for Numerical Methods in Engineering*, 79:1309 – 1331.
- Ladeira, I. (2023). *Development of a fast and reliable solver based on simplified formulae to assess the response of standalone tubular Offshore Wind Turbine supports subjected to ship impact*. PhD thesis, École centrale de Nantes.
- Ladeira, I., Echeverry, S., and Le Sourne, H. (2023). A simplified method to assess the elasto-plastic response of standalone tubular offshore wind turbine supports subjected to ship impact. *Ocean Engineering*, 279:114313.
- Le Sourne, H. (2007). A ship collision analysis program based on super-element method coupled with large rotational ship movement analysis. In *4th International Conference on Collision and Grounding of Ships*, pages 131–138.
- Mandra, J. O. (2023). Cargo ship strikes turbine at orsted's gode wind 1 offshore wind farm, suffers massive damage.
- Margientimmer (2022). Rudderless Julietta D causes damage to foundation of wind farm Hollandse Kust Zuid - Windpark Hollandse Kust South.
- Márquez, L., Le Sourne, H., and Rigo, P. (2022). Mechanical model for the analysis of ship collisions against reinforced concrete floaters of offshore wind turbines. *Ocean Engineering*, 261:111987.
- Ng, C. and Ran, L. (2016). *Offshore wind farms: Technologies, design and operation*. Woodhead Publishing.
- NORSOK (2012). Standard N-001. “Integrity of offshore structures”.

Bibliography

- Salazar L, P., Vandegar, G., Sone Oo, Y. P., Ladeira, I., Le Sourne, H., and Rigo, P. (2024). Simplified structural assessment of ship collision against a semisubmersible offshore wind floater. *Proceedings of The 34th (2024) International Ocean and Polar Engineering Conference, Rhodes, Greece.*
- Tong, W. (2010). *Wind power generation and wind turbine design.* WIT press.
- Travanca, J. and Hao, H. (2014). Dynamics of steel offshore platforms under ship impact. *Applied Ocean Research*, 47:352–372.
- Vandegar, G., Sone Oo, Y. P., Ladeira, I., Le Sourne, H., and Echeverry, S. (2023). A simplified method to assess the elastoplastic response of standalone tubular floating offshore wind turbine supports subjected to ship impact. *Proceedings of the International Conference on Collision and Grounding of Ships and Offshore Structures, Nantes, France.*
- Vaswani, A., Shazeer, N., Parmar, N., Uszkoreit, J., Jones, L., Gomez, A. N., Kaiser, L., and Polosukhin, I. (2017). Attention is all you need. *CoRR*, abs/1706.03762.
- Veritas, D. N. (2010). Design against accidental loads. *Recommended Practice DNV-RP-C204.*
- Yu, Z. and Amdahl, J. (2018). A review of structural responses and design of offshore tubular structures subjected to ship impacts. *Ocean Engineering*, 154(November 2017):177–203.
- Yu, Z., Amdahl, J., Rypestøl, M., and Cheng, Z. (2022). Numerical modelling and dynamic response analysis of a 10 mw semi-submersible floating offshore wind turbine subjected to ship collision loads. *Renewable Energy*, 184:677–699.
- Zhang, Y., Hu, Z., Ng, C., Jia, C., and Jiang, Z. (2021). Dynamic responses analysis of a 5 mw spar-type floating wind turbine under accidental ship-impact scenario. *Marine Structures*, 75:102885.